

# Sammba-MRI: a library for processing SmAll MaMmals BrAin MRI data in Python

Salma Bougacha<sup>1,2,3,4</sup>, Nachiket A. Nadkarni<sup>1,2</sup>, Marina Celestine<sup>1,2</sup>, Clément M. Garin<sup>1,2</sup>, and Marc Dhenain<sup>1,2,\*</sup>

<sup>1</sup>UMR9199 Laboratory of Neurodegenerative Diseases Mechanisms, Centre National de la Recherche Scientifique (CNRS), Fontenay-aux-Roses, France

<sup>2</sup>MIRcen, Institut François Jacob, Commissariat à l’Energie Atomique et aux Energies Alternatives (CEA), Fontenay aux Roses, France

<sup>3</sup>UMR-S U1237 Physiopathologie et imagerie des troubles Neurologiques (PhIND), INSERM, Université de Caen-Normandie, GIP Cyceron, Caen, France

<sup>4</sup>Normandie Université, UNICAEN, PSL Research University, EPHE, Inserm, U1077, CHU de Caen, Neuropsychologie et Imagerie de la Mémoire Humaine, Caen, France

Correspondence\*:

Marc Dhenain, MIRcen, UMR CEA-CNRS 9199, 18 Route du Panorama, 92265 Fontenay-aux-Roses CEDEX, France  
marc.dhenain@cea.fr

## 1 ABSTRACT

Small mammals neuroimaging offers incredible opportunities to investigate structural and functional aspects of the brain. Many tools have been developed in the last decade to analyse small animal data, but current software~~s~~ are less mature than the available tools that process human brain data. The Python package Sammba-MRI (SmAll MaMmals BrAin MRI in Python; <http://sambba-mri.github.io>) is designed to allow flexible and efficient use of existing methods and enables fluent scriptable analysis workflows, from raw data conversion to multimodal processing.

Keywords: Processing pipeline, MRI, registration, small animal Neuroimaging, Python

## 1 INTRODUCTION

The use of magnetic resonance imaging (MRI) methods in animals provides considerable benefits for improving our understanding of the brain structure and functioning in health and disease. The greatest advantages of preclinical MRI include group homogeneity and the opportunity to acquire a high amount of information repeated or modulated as needed. This added value, together with practical

and ethical considerations, resulted in an increase of the use of small mammals MRI in research. However, while human brain imaging benefits from a large variety of high level software solutions for MRI preprocessing and analysis, preclinical MRI is left behind. There is currently an urgent need for efficient and collaborative tools that would facilitate the adoption and dissemination of standardized pre-processing strategies for small animal MRI.

## 2 TOOLS: PYTHON ECOSYSTEM AND NEUROIMAGING SOFTWARE PACKAGES

With its Free and Open Source Software (FOSS) dependency stack and its growing neuroimaging community Python has been naturally the language of choice for our package. The scientific Python libraries used in Sammba-MRI are NumPy (Oliphant, 2006), SciPy (Millman and Aivazis, 2011), the neuroimaging data analysis tools nibabel<sup>1</sup>, Nilearn (Abraham et al., 2014) and Nipype (Gorgolewski et al., 2011). Visualization functionality depends on Matplotlib (Hunter, 2007) or Graphviz (Gansner and North, 2000), but neither is required to perform MRI data processing.

<sup>1</sup> <https://nipy.org/nibabel/>

Via Nipype, we utilize basic MRI preprocessing functions from AFNI (Cox, 1996), FSL (Jenkinson et al., 2012) and ANTs (Avants et al., 2009) packages. The dependency on the efficient but non open-source brain segmentation RATS tool (Oguz et al., 2014) is optional.

### 3 CODE DESIGN

Coding guidelines follow the model of Nilearn and other successfully adopted packages (e.g. Scikit-learn Pedregosa et al., 2011) to make the codebase understandable and easily maintainable<sup>2</sup>. Objects are used with parsimony : the different registration classes share all the same interface, and the brain extraction classes comply to the Nipype BaseInterface. Effort is made to keep the code uniformly formatted and to use consistent naming for the functions and parameters following the coding conventions of Nilearn. Preprocessing building blocks and pipelines are automatically tested on light MRI data samples to ensure code quality. Finally, the user is guided through Sammba-MRI with extensive documentation including installation instructions, API reference, pipelines graphs, and practical examples based on publicly available small animal neuroimaging datasets.

### 4 PREPROCESSING BRICKS

In this section, we provide a detailed explanation of the preprocessing building blocks (Figure 1).

#### 4.1 DICOM to NIfTI conversion

Sammba-MRI allows to convert Bruker DICOM (digital imaging and communications in medicine) files to the standard Neuroimaging Informatics Technology Initiative format (NIFTI-1) and extracts extensive information using DCMTK package (Eichelberg et al., 2004). Bruker files conversion is an active development field, with various available tools handling DICOM (e.g. dicomifier<sup>3</sup>) or not (e.g. bru2nii<sup>4</sup>, Bruker2nifti<sup>5</sup>, bru2nifti<sup>6</sup>).

<sup>2</sup> <http://gael-varoquaux.info/programming/software-design-for-maintainability.html>

<sup>3</sup> <https://github.com/lamyj/dicomifier>

<sup>4</sup> <https://github.com/neurolabusc/Bru2Nii>

<sup>5</sup> <https://github.com/CristinaChavarrias/Bruker2nifti>

<sup>6</sup> <https://github.com/SebastianoF/bru2nifti>

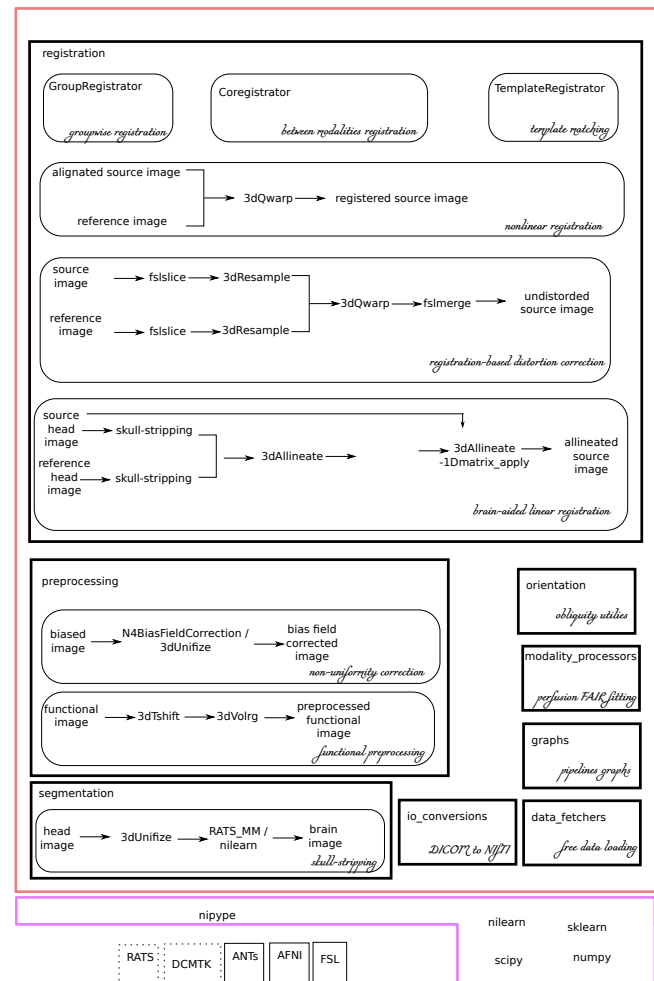


Figure 1. Sammba-MRI major modules.

Finally, ParaVision 360 with the latest patch 1.1 can export the NIFTI format since February 2019. Our implementation is meant to be a light helper function, allowing to handle the conversion on the fly. It has been tested only for Paravision 6 and a limited number of imaging sequences.

#### 4.2 Bias field correction

Intensity non-uniformity modelling is essential in preclinical studies because the intensity gradient corrupting MR images becomes particularly pronounced at high field strengths (Boyes et al., 2008). Sammba-MRI relies on AFNI’s 3dUnifize to correct for intensity bias in anatomical images, and on N4BiasFieldCorrection function of the ANTs package (Tustison et al., 2010) for the other modalities. 3dUnifize is also used to aid brain extraction, as detailed in the following paragraph.

### 4.3 Skull-stripping

Skull-stripping is the critical early step in processing MRI images from small animals. Various automatic rodent-specific software (Chou et al., 2011; Oguz et al., 2014) or adaptations of human algorithms (Wood et al., 2013; AFNI’s 3dskullstrip -rat) are freely available for research purposes. We choose to rely on the LOGISMOS-based graph segmentation (Yin et al., 2010) based on gray-scale mathematical morphology RATS software (Oguz et al., 2014) because of its good performance across a wide range of datasets (Sargolzaei et al., 2018). An alternative to the free but non-open source RATS tool is also available, based on an adaptation of the human histogram-based brain extraction method of Nilearn. This method can be used in any pipeline by setting the parameter use\_rats\_tool to False. Because intensity inhomogeneity can hamper the performance of automatic skull stripping, prior bias field correction is usually recommended (Sled et al., 1998) and is performed by default with 3dUnifize. The helper function brain\_segmentation\_report from Sambba-MRI segmentation module allows to efficiently tune the initial intensity threshold used in bias correction by producing for a given set of thresholds 5 informative measures characterizing the extracted mask to bypass time consuming repetitive visual checks. The returned features consist of the total volume of the extracted mask, its anteroposterior length, its right-left width, and its inferior-superior height as well as the sample Pearson’s product-moment correlation coefficient between the brain mask image and its reflection with respect to the estimated mid-sagittal plane (Powell et al., 2016).

## 5 READY-TO-USE PIPELINES

Sambba-MRI proposes optimized pipelines to perform spatial registration to a population or standard reference template, inter-modalities registration and functional and perfusion MRI processing. State-of-the-art small animal registration pipelines available as FOSS are the Atlas-based Imaging Data Analysis of structural and functional mouse

brain MRI (AIDAmri) (Pallast et al., 2019) package for the registration of functional and diffusion mouse brain MRI with the Allen Brain Reference atlas and the mouse-brain-optimized registration workflow (Ioanas et al., 2019) part of SAMRI package. Sambba-MRI pipelines have been tested throughout the different stages of their development process on various datasets from mouse, rat and mouse lemur and used in several publications from our lab (Garin et al., 2018; Nadkarni et al., 2019; Garin et al., 2019). All pipelines start with bias field correction for the individual images. The registration itself relies on AFNI’s 3dAllineate and 3dQwarp functions to estimate linear and non-linear (piecewise polynomial  $C^1$  diffeomorphism) transforms respectively between the source image and the reference image. Internal parameters of these functions have been optimized for small animal brains. We experienced a better performance when linear registration is performed on brain extracted images and nonlinear warps are computed using whole head images, and therefore followed this strategy across all the registration pipelines.

### 5.1 Template matching

Template matching is a necessary step for group studies. Several reference templates exist both for mouse and rat brains and the user needs to specify the path to the template of his choice to the TemplateRegistrar class from the registration module.

```
from sambba.registration import
    TemplateRegistrar
registrator = TemplateRegistrar(
    'dorr_t2.nii.gz',
    brain_volume=400)
registrator.fit('mouse01_t1.nii.gz')
```

We evaluated the registration accuracy of the proposed pipeline on the publicly available Brookhaven in vivo dataset, consisting of T2-weighted images of 12 C57BL/6J male adult mice and their segmentations in 20 brain regions (Ma et al., 2008). The scans were acquired using a 9.4 T Bruker scanner at 100  $\mu$ m isotropic resolution. The public dataset had

incomplete files/segmentations for 2 subjects so the evaluation was limited to 10 subjects. Because the shared individual images have been pre-registered to one reference image, we submitted them to slight random quadratic deformations (Normally distributed coefficients with  $\text{std}=0.1$  mm for translation,  $0.1$  degrees for rotation,  $0.02$  mm for scaling,  $0.02$  mm for shear and  $0.005$  mm for the remaining 31 polynomial coefficients) before performing the registration to the template. We then measured the regional overlap between each region in the average atlas and the transformed mice atlases using Dice similarity coefficient ( $2 \frac{|A \cap B|}{|A| + |B|}$ ). For comparison purposes, the registration was also performed using SPM mouse (Sawiak et al., 2009). Figure 2 shows that Sammba-MRI pipeline achieves high overlap values and outperforms SPM mouse in the majority of cases.

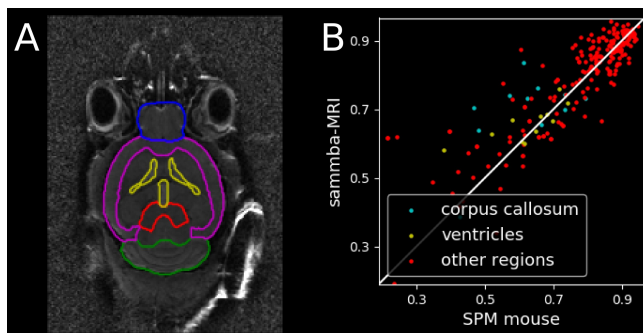


**Figure 2.** Registration to template of 10 C57 mice: (A) individual mouse anatomical image registered to the template with the contours of the average atlas superimposed as coloured lines; (B) Dice coefficient between each region in the average atlas and the transformed mice atlases (per region and animal).

## 5.2 Group-wise registration

Group-wise registration aims to align all images within a common space, resulting in an average brain that represents the commonalities among individual brain anatomies of a particular population. The use of cohort-specific templates eliminates possible bias toward external features and improves subsequent analyzes (De Feo and Giove, 2019). Sammba-MRI implements the multi-level, iterative scheme proposed by (Kovačević et al., 2005)

to create a fine anatomical template from individual structural MRI scans. A first rough template is obtained by averaging bias corrected head images centred on their respective brain masks barycentres. Then the individual images are registered to this template. This process of successive averaging/registration is iterated while increasing the number of degrees of freedom of the estimated transform and updating the target template (see (Nadkarni et al., 2019) for a detailed description of the pipeline). The method adapts to different small animal species, e.g. mouse lemurs (Nadkarni et al., 2018), and allows the creation of high quality group average templates (Figure 3).

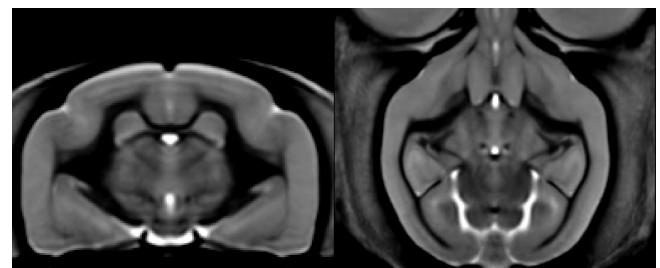


**Figure 3.** Mouse lemur template from 34 animals.

## 5.3 Multi-modal processing

In the context of the increasing use of multimodal imaging, several MRI techniques can be acquired from small animals, including structural imaging with different contrasts, blood-oxygenation-level-dependent (BOLD) and arterial spin labeling (ASL) MRI. In addition to the inherent difficulties in intermodality registration (Ashburner and Friston, 1997), severe image artifacts can corrupt the non-anatomical scan resulting in a low signal-to-noise ratio (SNR). For instance, the echo planar imaging (EPI) technique widely used in functional MRI and perfusion imaging suffers nonlinear geometric and intensity distortions caused by static magnetic field inhomogeneity that worsen at higher field strengths and have a more dramatic impact on small brains (Hong et al., 2015).

Intra-subject registration between an anatomical scan and another modality is handled through the



239 Coregistrato class from the registration  
240 module.

```
from sammba.registration import
    Coregistrato
coregistrato = Coregistrato(
    brain volume =400)
```

### 241 5.3.1 Rigid-body registration

242 Since orientation is correctly handled through the  
243 DICOM to NIfTI conversion, the anatomical image  
244 is first reoriented to match the modality of interest.  
245 Both images then undergo intensity unification and  
246 brain extraction. A rigid body transform that min-  
247 imizes normalized mutual information between the  
248 brain extracted images is finally estimated and ap-  
249 plied to the whole head images.

```
coregistrato.fit_anat(
    'mouse01_t1.nii.gz')
coregistrato.fit_modality(
    'mouse01_t2.nii.gz')
```

### 250 5.3.2 Reorientation-only

251 It is possible that the source or/and the reference  
252 images are of insufficient quality to correctly estim-  
253 ate a rigid body transform. In this case, assuming  
254 that the head motion between the two acquisitions  
255 is low, it is better to only reorient the anatomical  
256 image to match the modality of interest.

```
coregistrato.fit_anat(
    'mouse01_t1.nii.gz')
coregistrato.fit_modality(
    'mouse01_t2.nii.gz',
    reorient_only=True)
```

### 257 5.3.3 Resting state BOLD fMRI processing

258 BOLD scans are preprocessed using the same  
259 usual steps for human data with optional slice tim-  
260 ing correction, bias field correction, realignment to  
261 the first volume and computation of the temporal  
262 mean of all the volumes. The corresponding struc-  
263 tural scan is then registered to the average BOLD  
264 scan. Since this is a critical step, the user can  
265 choose either to pursue with human-like pipeline

by estimating a rigid body functional-to- structural 266  
transform and applying its inverse to the structural 267  
image, or to assume that the head motion between 268  
the two scans is negligible. In all cases, the trans- 269  
formed or not structural image is then reoriented to 270  
match the functional image. Next, the average func- 271  
tional image and the reoriented structural image are 272  
split into 2D slices along the z-direction (accord- 273  
ing to the slice geometry of the functional image) 274  
and each functional slice undergoes afterwards a 275  
nonlinear registration step to best match the corres- 276  
ponding structural slice. This per-slice registration 277  
corrects for EPI distortion while being more conser- 278  
vative than a global 3D nonlinear registration, to 279  
better manage large slice thickness in the BOLD 280  
acquisitions of small animals. Since geometric dis- 281  
tortions are higher in the through plane direction 282  
due to the typically lower resolution than in- plane, 283  
the correction is still satisfactory. 284

### 5.3.4 ASL fMRI processing 285

ASL is an attractive method to image the vascular 286  
system by directly measuring blood flow. However, 287  
estimating the cerebral blood flow (CBF) in small 288  
animals is challenging due to the low SNR and lack 289  
of sensitivity (Kober et al., 2008). Sammba-MRI al- 290  
lows to preprocess functional ASL scans with the 291  
M0 scan used as the representative volume for re- 292  
gistration. No between volume realignment is per- 293  
formed because of the usual poor SNR. For Bruker- 294  
FAIR (Flow-sensitive Alternating Inversion Recov- 295  
ery) EPI sequences, quantitative CBF maps can be 296  
estimated using fair\_to\_proc function from the 297  
modality\_processor module. 298

### 5.4 Modality to template and vice versa 299

BOLD and ASL preprocessing can be performed 300  
in the individual space with Coregistrato or 301  
in template space with TemplateRegistrato. In 302  
the latter case, the structural-to-template warp, the 303  
functional-to-structural rigid body transform and 304  
the perslice functional-to-structural warps are com- 305  
bined and applied in a one-big-step transformation 306  
to the functional data to minimize interpolation 307  
errors. The TemplateRegistrato class encom- 308  
passes an inverse\_transform\_towards\_modality 309

method to bring an image from the reference space to the individual's space.

## 5.5 Results

Resting state fMRI allows to study temporally synchronized BOLD oscillations reflecting functionally connected brain networks. As in human resting state fMRI, spatial networks can be extracted using Independent Components Analysis (ICA) and were successfully demonstrated in anaesthetized mice (Zerbi et al., 2015; Grandjean et al., 2019). We preprocessed the publicly shared functional data from 15 mice (2-3 months old) from Zerbi et al. (2015) paper with Sambba-MRI and performed a group ICA (Varoquaux et al., 2010) with 30 components. Relevant bilateral regions related to somatosensory, hippocampal, visual, basal ganglia, and sensorimotor networks. were obtained without additional data post-processing Figure 4. To illustrate the perfusion processing pipeline, we used perfusion FAIR images from 10 C57BL/6J mice (5-7 months) to quantify CBF. Figure 5 shows voxelwise map averaged across all individuals and regional absolute CBF values, all in agreement with the literature (Muir et al., 2008).

## 6 BIG DATA, REPRODUCIBILITY, COLLABORATION

The package design facilitates big data exploration: the user is able to run an entire analysis in a single Python script, rerunning pipelines is optimized through Nipype caching mechanism and long lasting steps (nonlinear warping, perfusion fitting) are executed in parallel. We believe that reproducibility in the neuroimaging field is not possible without making the acquired images and the preprocessing code available to the community. For this reason, Sambba-MRI promotes the sharing of MRI data by providing utility functions to download public small animal brain MRI datasets and relies on it for demoing the package capabilities. In order to encourage external contributions, our library source code is hosted on the open collaborative GitHub platform and distributed under the CeCILL v2.1 license, a FOSS license adapted to both international and French legal matters allowing anyone to make

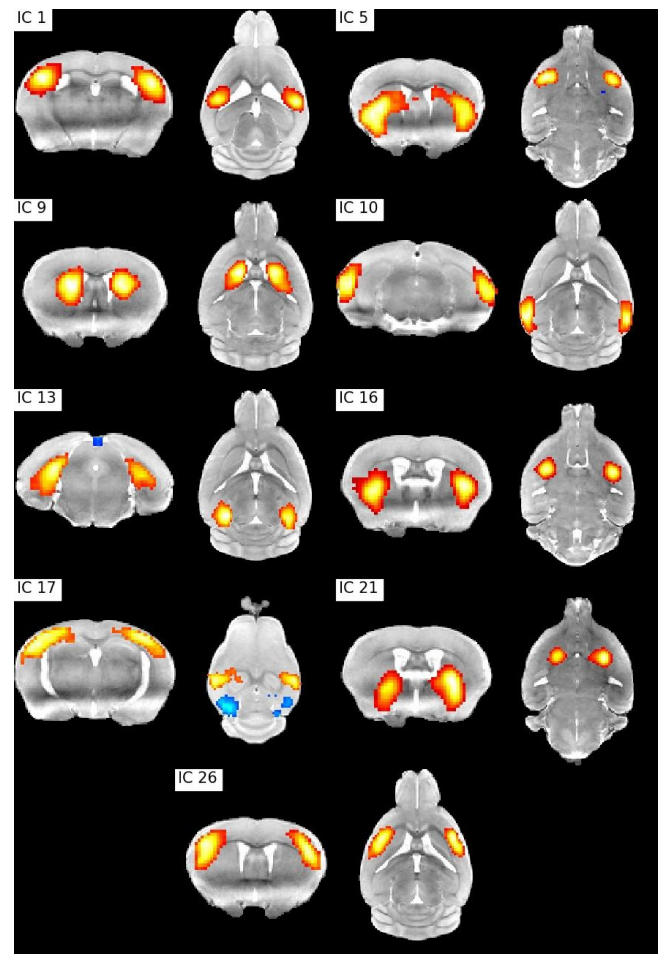


**Figure 4.** ICA bilateral components. IC 1: Barrel field (i) cortex, IC 5: Lateral striatum, IC 9: Dorsal striatum (i), IC 10: Visual cortex, IC 13: Hippocampus, IC 16: Dorsal striatum (ii), IC 17: Barrel field (ii) cortex, IC 21: Ventral striatum, IC 26: Supplementary cortex

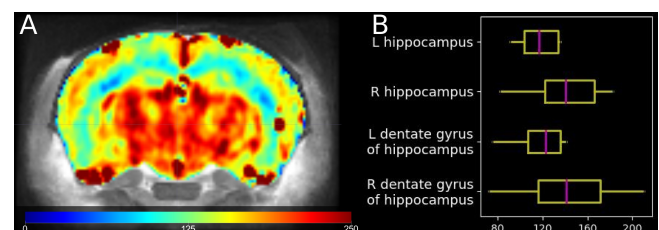


**Figure 5.** CBF from 10 C57 mice in ml/100g/min: (A) group average CBF map ; (B) individual regional CBF.

changes and redistribute it. Sambba-MRI supports GNU/Linux and Mac OS X operating systems (OS), used by over 70% of neuroimagers (Hanke and Halchenko, 2011).

## 7 CONCLUSION

By efficiently combining different existing human and animal neuroimaging tools, Sammba-MRI allows to tackle common processing issues in a fully automated fashion. High quality spatial registration can be easily performed, including template matching, between modalities registration as well as the creation of cohort-specific templates. Sammba-MRI also implements functional and perfusion MRI preprocessing methods and cerebral blood flow estimation for FLAIR perfusion images. Emphasis is put on code readability and ease of use to favour contributions from the community.

## CONFLICT OF INTEREST STATEMENT

The authors declare that the research was conducted in the absence of any commercial or financial relationships that could be construed as a potential conflict of interest.

## AUTHOR CONTRIBUTIONS

SB, NN and MC contributed code to the project. NN, CG and MD contributed to data acquisition. SB wrote the manuscript with input from CG and NN. Every author read and approved the manuscript.

## FUNDING

We thank the France-Alzheimer Association, Plan Alzheimer Foundation and the French Public Investment Bank’s “ROMANE” program for funding this study.

## DATA AVAILABILITY STATEMENT

The mouse lemur dataset can be automatically loaded through Sammba-MRI or directly from <https://nitrc.org/projects/mouselemuratlas> for the template and <https://openneuro.org/datasets/ds001945> for the original anatomical images. The perfusion dataset will be made publicly available following publication.

## REFERENCES

- Abraham, A., Pedregosa, F., Eickenberg, M., Ger-  
vais, P., Mueller, A., Kossaifi, J., et al. (2014).  
Machine learning for neuroimaging with scikit-  
learn. *Frontiers in neuroinformatics* 8, 14. doi:10.3389/fninf.2014.00014
- Ashburner, J. and Friston, K. (1997). Multimodal  
image coregistration and partitioning—a unified  
framework. *NeuroImage* 6, 209–217. doi:10.1006/nimg.1997.0290
- Avants, B. B., Tustison, N., and Song, G. (2009).  
Advanced normalization tools (ANTS). *Insight*  
*J* 2, 1–35
- Boyes, R. G., Gunter, J. L., Frost, C., Janke, A. L.,  
Yeatman, T., Hill, D. L., et al. (2008). In-  
tensity non-uniformity correction using N3 on  
3-T scanners with multichannel phased array  
coils. *NeuroImage* 39, 1752–1762. doi:10.1016/j.neuroimage.2007.10.026
- Chou, N., Wu, J., Bingren, J. B., Qiu, A., and  
Chuang, K.-H. (2011). Robust automatic rodent  
brain extraction using 3-D pulse-coupled neural  
networks (PCNN). *IEEE Transactions on Im-  
age Processing* 20, 2554–2564. doi:10.1109/TIP.2011.2126587
- Cox, R. W. (1996). AFNI: software for analysis  
and visualization of functional magnetic reson-  
ance neuroimages. *Computers and Biomedical  
research* 29, 162–173. doi:10.1006/cbmr.1996.0014
- De Feo, R. and Giove, F. (2019). Towards an effi-  
cient segmentation of small rodents brain: a short  
critical review. *Journal of Neuroscience Meth-  
ods* 323, 82–89. doi:10.1016/j.jneumeth.2019.05.003
- Eichelberg, M., Riesmeier, J., Wilkens, T., Hewett,  
A. J., Barth, A., and Jensch, P. (2004). Ten  
years of medical imaging standardization and  
prototypical implementation: the DICOM stand-  
ard and the OFFIS DICOM toolkit (DCMTK). In  
*Medical Imaging 2004: PACS and Imaging In-  
formatics* (International Society for Optics and  
Photonics), vol. 5371, 57–69



- 430 Gansner, E. R. and North, S. C. (2000). An  
431 open graph visualization system and its ap-  
432 plications to software engineering. *Soft-*  
433 *ware: practice and experience* 30, 1203–  
434 1233. doi:10.1002/1097-024X(200009)30:  
435 11<1203::AID-SPE338>3.0.CO;2-N
- 436 Garin, C. M., Nadkarni, N. A., Bougacha, S.,  
437 Picq, J.-L., Pepin, J., Flament, J., et al. (2018).  
438 Resting state, gluCEST and anatomical MRI ap-  
439 proaches at 11.7T for brain aging studies in a  
440 non-human primate. In *Joint Annual Meeting*  
441 *ISMRM-ESMRMB 2018*
- 442 Garin, C. M., Nadkarni, N. A., Landeau, B., Chet-  
443 elat, G., Picq, J.-L., Bougacha, S., et al. (2019).  
444 Resting state cerebral networks in mouse lemur  
445 primates: from multilevel validation to compar-  
446 ison with humans. doi:10.1101/599423. Pre-  
447 print
- 448 Gorgolewski, K., Burns, C. D., Madison, C., Clark,  
449 D., Halchenko, Y. O., Waskom, M. L., et al.  
450 (2011). Nipype: a flexible, lightweight and  
451 extensible neuroimaging data processing frame-  
452 work in python. *Frontiers in neuroinformatics* 5,  
453 13. doi:10.3389/fninf.2011.00013
- 454 Grandjean, J., Canella, C., Anckaerts, C., Ayranci,  
455 G., Bougacha, S., Bienert, T., et al. (2019).  
456 Common functional networks in the mouse brain  
457 revealed by multi-centre resting-state fMRI ana-  
458 lysis
- 459 Hanke, M. and Halchenko, Y. O. (2011). Neur-  
460 oscience runs on GNU/Linux. *Frontiers in*  
461 *Neuroinformatics* 5, 8. doi:10.3389/fninf.2011.  
462 00008
- 463 Hong, X., To, X. V., Teh, I., Soh, J. R., and Chuang,  
464 K.-H. (2015). Evaluation of EPI distortion cor-  
465 rection methods for quantitative MRI of the brain  
466 at high magnetic field. *Magnetic resonance ima-*  
467 *ging* 33, 1098–1105. doi:10.1016/j.mri.2015.06.  
468 010
- 469 Hunter, J. D. (2007). Matplotlib: A 2D graphics en-  
470 vironment. *Computing in science & engineering*  
471 9, 90. doi:10.1109/MCSE.2007.55
- 472 Ioanas, H.-I., Marks, M., Yanik, M. F., and Rudin,  
473 M. (2019). An Optimized Registration Work-  
474 flow and Standard Geometric Space for Small  
Animal Brain Imaging. Preprint 475
- Jenkinson, M., Beckmann, C. F., Behrens, T. E., 476  
Woolrich, M. W., and Smith, S. M. (2012). 477  
Fsl. *NeuroImage* 62, 782–790. doi:10.1016/j. 478  
neuroimage 479
- Kober, F., Duhamel, G., and Cozzone, P. J. (2008). 480  
Experimental comparison of four FAIR arter- 481  
ial spin labeling techniques for quantification of 482  
mouse cerebral blood flow at 4.7 T. *NMR in* 483  
*Biomedicine: An International Journal Devoted* 484  
*to the Development and Application of Magnetic* 485  
*Resonance In vivo* 21, 781–792. doi:10.1002/ 486  
nbm.1253 487
- Kovačević, N., Henderson, J., Chan, E., Lifshitz, 488  
N., Bishop, J., Evans, A., et al. (2005). A three- 489  
dimensional MRI atlas of the mouse brain with 490  
estimates of the average and variability. *Cereb-* 491  
*ral Cortex* 15, 639–645. doi:10.1093/cercor/ 492  
bhh165 493
- Ma, Y., Smith, D., Hof, P. R., Foerster, B., 494  
Hamilton, S., Blackband, S. J., et al. (2008). 495  
In vivo 3D digital atlas database of the adult 496  
C57BL/6J mouse brain by magnetic resonance 497  
microscopy. *Frontiers in neuroanatomy* 2, 1. 498  
doi:10.3389/neuro.05.001.2008 499
- Millman, K. J. and Aivazis, M. (2011). Python for 500  
scientists and engineers. *Computing in Science* 501  
*& Engineering* 13, 9–12. doi:10.1109/MCSE. 502  
2011.36 503
- Muir, E. R., Shen, Q., and Duong, T. Q. (2008). 504  
Cerebral blood flow MRI in mice using the 505  
cardiac-spin-labeling technique. *Magnetic Res-* 506  
*onance in Medicine* 60, 744–748. doi:10.1002/ 507  
mrm.21721 508
- [Dataset] Nadkarni, N. A., Bougacha, S., Garin, C., 509  
Dhenain, M., and Picq, J.-L. (2018). Digital tem- 510  
plates and brain atlas dataset for the mouse lemur 511  
primate. doi:10.1016/j.dib.2018.10.067 512
- Nadkarni, N. A., Bougacha, S., Garin, C., Dhenain, 513  
M., and Picq, J.-L. (2019). A 3D population- 514  
based brain atlas of the mouse lemur primate 515  
with examples of applications in aging studies 516  
and comparative anatomy. *NeuroImage* 185, 517  
85–95. doi:10.1016/j.neuroimage.2018.10.010 518



- 519 Oguz, I., Zhang, H., Rumple, A., and Sonka, M.  
520 (2014). RATS: Rapid Automatic Tissue Seg-  
521 mentation in rodent brain MRI. *Journal of Neur-*  
522 *oscience Methods* 221, 175–182. doi:10.1016/j.  
523 jneumeth.2013.09.021
- 524 Oliphant, T. E. (2006). *A guide to NumPy*, vol. 1  
525 (Trelgol Publishing USA)
- 526 Pallast, N., Diedenhofen, M., Blaschke, S.,  
527 Wieters, F., Wiedermann, D., Hoehn, M., et al.  
528 (2019). Processing pipeline for Atlas-based  
529 Imaging Data Analysis of structural and func-  
530 tional mouse brain MRI (AIDAmri). *Frontiers*  
531 *in Neuroinformatics* 13, 42. doi:10.3389/fninf.  
532 2019.00042
- 533 Pedregosa, F., Varoquaux, G., Gramfort, A.,  
534 Michel, V., Thirion, B., Grisel, O., et al.  
535 (2011). Scikit-learn: Machine learning in Py-  
536 thon. *Journal of Machine Learning Research* 12,  
537 2825–2830
- 538 Powell, N. M., Modat, M., Cardoso, M. J., Ma,  
539 D., Holmes, H. E., Yu, Y., et al. (2016). Fully-  
540 automated  $\mu$ MRI morphometric phenotyping of  
541 the Tc1 mouse model of Down syndrome. *PloS*  
542 *one* 11, e0162974
- 543 Sargolzaei, S., Cai, Y., Wolahan, S. M., Gaonkar,  
544 B., Sargolzaei, A., Giza, C. C., et al. (2018).  
545 A Comparative Study of Automatic Approaches  
546 for Preclinical MRI-based Brain Segmentation  
547 in the Developing Rat. In *2018 40th Annual*  
548 *International Conference of the IEEE Engineer-*  
549 *ing in Medicine and Biology Society (EMBC)*  
550 (IEEE), 652–655
- 551 Sawiak, S., Wood, N., Williams, G., Morton, A.,  
552 and Carpenter, T. (2009). SPMMouse: A new  
553 toolbox for SPM in the animal brain. In *ISMRM*  
554 *17th Scientific Meeting & Exhibition, April*. 18–  
555 24
- 556 Sled, J. G., Zijdenbos, A. P., and Evans, A. C.  
557 (1998). A nonparametric method for automatic  
558 correction of intensity nonuniformity in MRI  
559 data. *IEEE transactions on medical imaging* 17,  
560 87–97
- 561 Tustison, N. J., Avants, B. B., Cook, P. A., Zheng,  
562 Y., Egan, A., Yushkevich, P. A., et al. (2010).  
563 N4ITK: improved N3 bias correction. *IEEE*  
*transactions on medical imaging* 29, 1310 564
- Varoquaux, G., Sadaghiani, S., Pinel, P., Kleinsch- 565  
midt, A., Poline, J.-B., and Thirion, B. (2010). 566  
A group model for stable multi-subject ICA on 567  
fMRI datasets. *Neuroimage* 51, 288–299 568
- Wood, T. C., Lythgoe, D. J., and Williams, S. C. 569  
(2013). rBET: making BET work for rodent 570  
brains. In *Proc. Intl. Soc. Mag. Reson. Med.* 571  
vol. 21, 2706 572
- Yin, Y. et al. (2010). LOGISMOS - Layered 573  
Optimal Graph Image Segmentation of Multiple 574  
Objects and Surfaces: cartilage segmentation in 575  
the knee joint. *IEEE Trans Med Imaging* 576
- Zerbi, V. et al. (2015). Mapping the Mouse Brain 577  
with Rs-fMRI: An Optimized Pipeline for Func- 578  
tional Network Identification. *NeuroImage* 123, 579  
11–21 580

